Accelerating ordered subsets image reconstruction for X-ray CT using spatially non-uniform optimization transfer: Supplementary material

Donghwan Kim, *Student Member, IEEE,* Debashish Pal, *Member, IEEE,* Jean-Baptiste Thibault, *Member, IEEE,* and Jeffrey A. Fessler, *Fellow, IEEE*

This material extends the result section of [1] by providing cost function plots and a simulation study of a helical scan of the XCAT phantom [2].

References to equations, tables, figures, bibliography are within this material unless they are specified.

I. Cost function

In [1], we computed root mean square difference (RMSD) within region-of-interest (ROI) to evaluate the convergence rate of the proposed algorithm. Another way to assess the convergence rate is computing the cost function $\Psi(x)$ in [1, Eqn. (2)] at each iteration. We used the following metric:

$$\xi^{(n)} = 20 \log_{10} \left(\frac{\Psi(x^{(n)}) - \Psi(x^{(\infty)})}{\Psi(x^{(\infty)})} \right) \text{ [dB]} \qquad (1)$$

to better visualize how the cost function decreases each iteration. We used double precision and triple **for** loops when accumulating $\Psi(x^{(n)})$ to ensure high accuracy.

Fig. 2 shows plots of $\xi^{(n)}$ for the choices of parameters used in [1, Fig. 5 and 6] for two real 3D scans; GE performance phantom (GEPP) and shoulder region scan. Fig. 2(a) shows that for the GEPP case, the NU-OS methods decreased the cost function at about the same rate than the ordinary OS method, or even perhaps slightly slower. In contrast, when we plotted RMSD distance to the converged image within the ROI [1, Fig. 5], NU-OS converged significantly faster. The reason for this different behavior is that the cost function plot considers all voxels, even those outside the ROI which are not of interest clinically. It is known that OS methods are not guaranteed to converge and apparently the non-ROI voxels are either not converging or perhaps approaching a larger limit-cycle, presumably due to the poor sampling in the padded slices outside the ROI, even with the stabilizing methods outside ROI described in [1, Section V]. Therefore, cost function plots may not provide practical measures of convergence rate for OS methods, particularly with acceleration. Future research on trying to further stabilize the NU-OS-SQS algorithm outside the ROI also may be helpful.

The final drops at the right in Fig. 2(a) show that averaging sub-iterations at the last iteration, as described in [1, Section IV.C], can compensate for the limit-cycle, particularly outside the ROI.

Unlike Fig. 2(a), the plots in Fig. 2(b) and 2(c) of shoulder region scan look similar to the plots of RMSD within ROI in [1, Fig. 6]. The scan geometry of each data set might explain these behavior of cost function in Fig. 2, where the shoulder region scan is a helical scan with pitch 1.0 and 7 helical turns and thus the corresponding image space has relatively few voxels outside the ROI, compared with GEPP data that is acquired by a helical scan with pitch 0.5 and 3 helical turns. Therefore, we can expect the cost function of shoulder region scan to be less affected by instability outside the ROI. Slower convergence of NU-OS-SQS algorithm at early iterations in Fig. 2(c) means that some choices of initial update-needed factor $\tilde{u}_j^{(0)}$ were not good enough for voxels outside the ROI. The effect of averaging at the last iterations is apparent in Fig. 2(b) and 2(c), because the instability outside the ROI is suppressed by the averaging.

II. Simulation data

A. Simulation data

We simulated a helical CT scan data by using XCAT phantom [2]. We first acquired a $1024 \times 1024 \times 154$ XCAT phantom for 500 [mm] transaxial field-of-view (FOV) at 70 [keV], where $\Delta_x = \Delta_y = 0.4883$ [mm] and $\Delta_z = 0.6250$ [mm]. (See Fig. 1.)

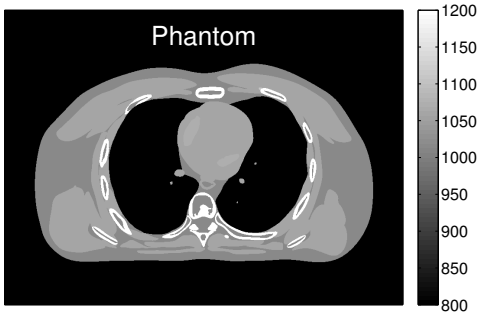

Fig. 1. A simulated XCAT phantom: a center slice of $1024 \times 1024 \times 154$ XCAT phantom. (Images are cropped for better visualization.)

Date of current version June 4, 2013. This work was supported in part by GE Healthcare, the National Institutes of Health under Grant R01-HL-098686, and equipment donations from Intel.

Donghwan Kim and Jeffrey A. Fessler are with the Department of Electrical Engineering and Computer Science, University of Michigan, Ann Arbor, MI 48105 USA (e-mail: kimdongh@umich.edu, fessler@umich.edu).

Debashish Pal and Jean-Baptiste Thibault are with GE Healthcare Technologies, 3000 N Grandview Blvd, W-1180, Waukesha, WI 53188 USA (e-mail: debashish.pal@ge.com, jean-baptiste.thibault@med.ge.com).

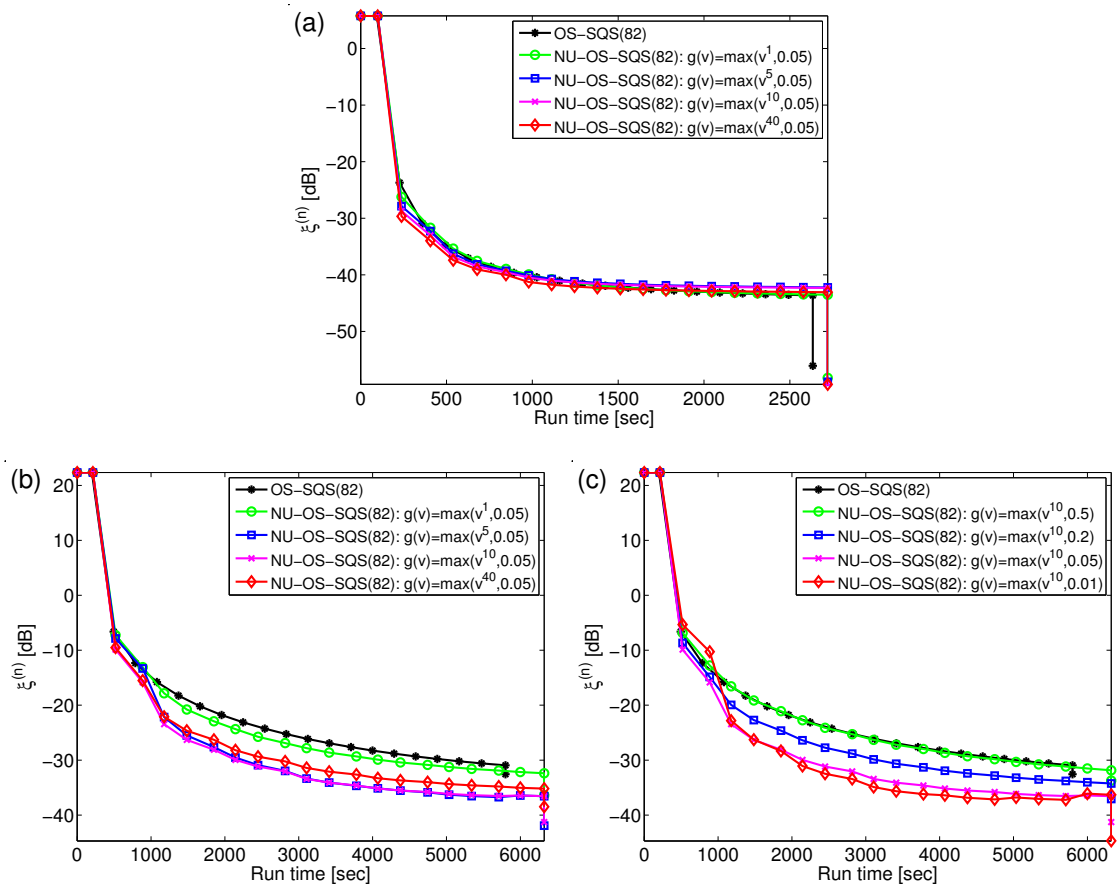

Fig. 2. Plots of $\xi^{(n)}$ in (1) as a function of run time for different choice of DRA parameters for (a) GE performance phantom and (b-c) a shoulder region scan.

We simulated a helical scan using the blank scan factor $b_i = 10^6$ and the mean number of background events $r_i = 0$ with Poisson noise. The sinogram data is in $888 \times 64 \times 2934$ (the number of detector columns$\times$detector rows$\times$projection views) space with pitch 1.0. Then, we reconstructed a $512 \times 512 \times 154$ image where $\Delta_x = \Delta_y = 0.9766$[mm] and $\Delta_z = 0.6250$[mm] using the proposed NU-OS-SQS algorithm.

B. Results

We use a cost function that is similar to the cost function used in [1, Section V]. We solve a PWLS function with a potential function $\psi_k(t) \triangleq \bar{\omega}_k \psi(t)$ in [1, Eqn. (45)] using a spatial weighting parameter:

$$\bar{\omega}_k \triangleq 50 \cdot \prod_{\substack{j=1 \\ c_{kj} \neq 0}}^{N_p} \max\{\kappa_j,\, 0.01\, \kappa_{\max}\} \qquad (2)$$

that provides uniform resolution properties [3], where

$$\kappa_j \triangleq \sqrt{\frac{\sum_{i=1}^{N_d} a_{ij} w_i}{\sum_{i=1}^{N_d} a_{ij}}} \qquad (3)$$

and the value of $\kappa_{\max} \triangleq \max_j \kappa_j$ is used in (2) to avoid under-regularizing some voxels with very small κ_j. Fig. 3 illustrates both RMSD within ROI and $\xi^{(n)}$ versus computation time, which we run the algorithm on the machine described in [1].

In Fig. 3(a), we evaluated the convergence rate using RMSD within ROI between current and converged image, where the converged image was generated by many iterations of a (convergent) SQS. We used parameters of DRA function that are used in [1, Fig. 5 and 6], and we observed similar trends. We also illustrate the plot of $\xi^{(n)}$ versus run time in Fig. 3(b), which looks very similar to Fig. 3(a). This is because we regularized relatively more than two other experiments in this simulation experiment, and thus instability outside the ROI that can be caused by NU-OS-SQS methods is not apparent here.

In Fig. 4(a), the reconstructed images of (NU-)OS-SQS show that NU method accelerates OS-SQS and reaches closer to the converged image after the same computation time (88 min.). This is apparent when comparing the difference images between the reconstructed and converged images in Fig. 4(b), particularly around the spine.

REFERENCES

[1] D. Kim, D. Pal, J-B. Thibault, and J. A. Fessler, "Accelerating ordered subsets image reconstruction for X-ray CT using spatially non-uniform optimization transfer," *IEEE Trans. Med. Imag.*, 2013, To appear.

[2] W. P. Segars, M. Mahesh, T. J. Beck, E. C. Frey, and B. M. W. Tsui, "Realistic CT simulation using the 4D XCAT phantom," *Med. Phys.*, vol. 35, no. 8, pp. 3800–8, Aug. 2008.

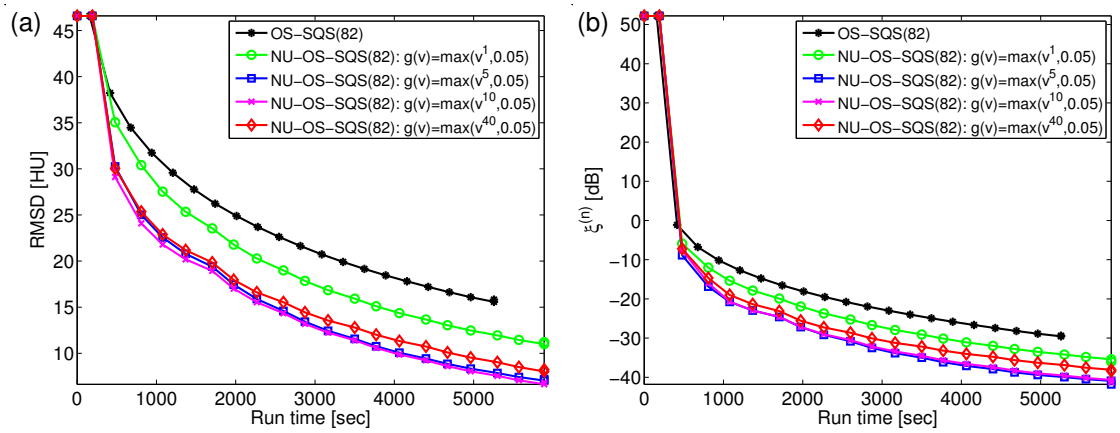

Fig. 3. A simulated XCAT phantom: plots of (a) RMSD and (b) $\xi^{(n)}$ versus run time for different choice of parameters t for $\epsilon = 0.05$ in $g(v) = \max\left\{v^t,\ \epsilon\right\}$.

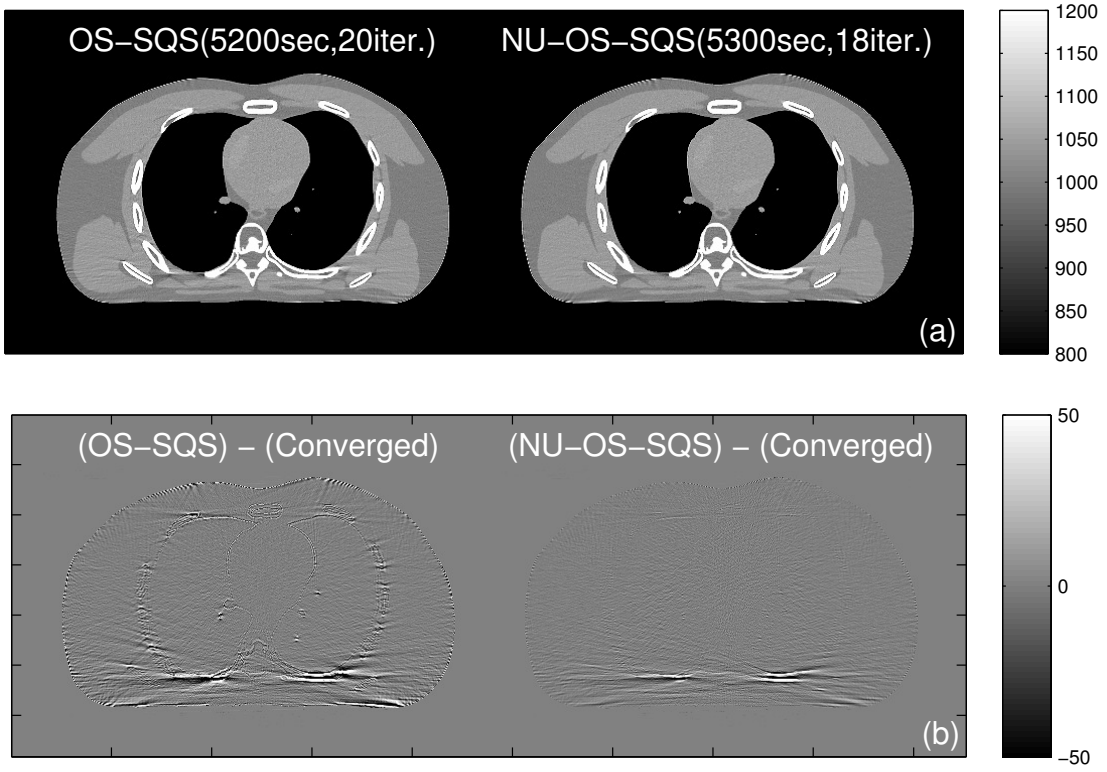

Fig. 4. A simulated XCAT phantom: (a) A center slice of reconstructed image by OS-SQS(82) and NU-OS-SQS(82)-$g(v) = \max\left\{v^{10},\ 0.05\right\}$ after about 88 min. (b) Difference between the reconstructed and converged images are additionally shown to illustrate the acceleration of NU approach. (Images are cropped for better visualization.)

[3] J. A. Fessler and W. L. Rogers, "Spatial resolution properties of penalized-likelihood image reconstruction methods: Space-invariant tomographs," *IEEE Trans. Im. Proc.*, vol. 5, no. 9, pp. 1346–58, Sept. 1996.